Title

Chemical Forms of Mercury in Pilot Whales Determined from Species-Averaged Mercury Isotope Signatures

Journal

ACS Earth and Space Chemistry, 5(6)

ISSN

2472-3452

Authors

Manceau, Alain
Brossier, Romain
Poulin, Brett A

Publication Date

2021-06-17

DOI

10.1021/acsearthspacechem.1c00082

Peer reviewed

Chemical Forms of Mercury in Pilot Whales Determined from Species-Averaged Mercury Isotope Signatures

Alain Manceau[1,*], Romain Brossier[1,*], and Brett A. Poulin[2]

[1]Université Grenoble Alpes, ISTerre, CNRS, 38000 Grenoble, France

[2]Department of Environmental Toxicology, University of California Davis, Davis, CA 95616, USA

Correspondence: alain.manceau@univ-grenoble-alpes.fr

ABSTRACT: Marine mammals detoxify organic methylmercury (MeHg) as inorganic mercury selenide (HgSe), yet the nature of the reaction intermediate species and the tissue-specific redistribution of Hg species in the body are unknown. We report that the identity and proportion of the dominant Hg species in long-finned pilot whale (*Globicephala melas*) tissues can be obtained from the bulk variation of isotopic values of δ^{202}Hg against the extent of demethylation (percentage of total Hg as MeHg, %MeHg) using an alternating regularized inversion method. Our analysis of isotope data from two previous studies supports that MeHg is demethylated as a tetraselenolate species ($Hg(Sec)_4$), which further transforms into HgSe. $Hg(Sec)_4$ occurs in the liver, kidneys, muscle, heart, and brain, whereas HgSe biomineralization occurs only in the liver and kidneys. This study provides a mathematical approach that facilitates probing the molecular-level chemistry of mercury in biological tissues using bulk isotopic data.

Keywords: Mercury, demethylation, isotope fractionation, whale, inversion

INTRODUCTION

The enrichment of the biosphere in anthropogenic mercury (Hg) impacts wildlife and humans across the globe.[1-4] Despite detailed understanding of the environmental conditions that promote the uptake of neurotoxic methylmercury (MeHg) in food webs, key knowledge gaps remain on the internal transformations, redistribution, and toxicologic mechanisms of Hg in higher organisms. Recently, advancement in the application of high energy-resolution X-ray absorption (HR-XANES) spectroscopy in wildlife identified that MeHg is detoxified to nontoxic mercury selenide (HgSe) through an intermediary Hg-tetraselenolate ($Hg(Sec)_4$) species.[5-7] The step-wise transformation of MeHg observed in bird and fish tissues (MeHg → $Hg(Sec)_4$ → HgSe), likely initiated by selenoprotein P (SelP),[5] provided the first *in vivo* mechanistic information for the observation of HgSe in the liver and extrahepatic tissues of marine mammals[8-12] and seabirds[6] using standard resolution X-ray absorption spectroscopy and electron microscopy. Although these two techniques provide critical structural information on mercury,[8-26] they provide limited insight into biochemical processes essential for understanding the toxicokinetics of toxic MeHg in organisms (i.e., fate, tissue-specific exchange).

Stable isotope ratios of Hg offer a powerful alternative to spectroscopic and microscopic approaches.[27] Chemical reactions induce a fractionation of isotopes between reactants and products,[28-34] and therefore Hg metabolic pathways can be investigated if species-specific stable isotope signatures are known.[35, 36] The isotopic fractionation of ^{202}Hg relative to ^{198}Hg (denoted as $\delta^{202}Hg$) is well suited for this purpose because $\delta^{202}Hg$ can vary by more than 3.5‰ in biological tissues.[30] However, tissues usually contain more than one Hg species,[5, 6] thus bulk $\delta^{202}Hg$ values are weighted averages of all $\delta^{202}Sp_i$ values present in the tissue

$$\delta^{202}Hg_t = \sum f(Sp_{i,t}) \times \delta^{202}Sp_i \quad (1)$$

where i is the number of species and $f(Sp_{i,t})$ is the molar fraction of species i in tissue t. At present, a key limitation in the field of Hg toxicology is resolving the linkages between the speciation of Hg and bulk $\delta^{202}Hg$ values.

The first attempt to combine HR-XANES spectroscopy and ^{202}Hg fractionation was performed recently by Poulin et al.[37] on piscivorous birds from lacustrine, estuarine, and marine environments. The demethylation of MeHg to $Hg(Sec)_4$ led to a $\delta^{202}Hg(Sec)_4$ - $\delta^{202}MeHg$ = -2.2 ± 0.1‰ depletion of the ^{202}Hg isotope. Here, we follow a different approach and show that the isotopic signature and proportion of unique Hg species ($\delta^{202}Sp_i$ and $f(Sp_{i,t})$) can be obtained directly from bulk $\delta^{202}Hg_t$ values of tissues and the molar fraction of MeHg to total Hg (f(MeHg)), the latter being a routine chemical measurement. The demonstration is performed on two independent data sets on long-finned pilot whale (*Globicephala melas*) tissues documented by Li et al. (2020)[36] and Bolea-Fernandez et al. (2019)[38]. The speciation of Hg as MeHg, $Hg(Sec)_4$, and HgSe in long-finned pilot whale tissues were obtained by calculating iteratively the isotopic signature and proportion of unique Hg species ($\delta^{202}Sp_i$ and $f(Sp_{i,t})$) using a regularized inversion method.[39, 40] The mathematical approach showcases how Hg speciation data can be obtained from bulk isotopic ratios, providing a new tool to investigate the transformations and tissue-specific redistribution of the Hg species in organisms.

METHODS

Data. The $\delta^{202}Hg_t$, $[Hg]_{tot}$, total Se ($[Se]_{tot}$), and f(MeHg) data from Li et al. (2020)[36] included data of the liver, kidneys, muscle, heart, and brain of 3 juvenile and 4 adult long-finned pilot whales (*G. melas*) sampled in the Faroe Islands (2016) (n = 35). The $\delta^{202}Hg_t$, $[Hg]_{tot}$, and f(MeHg) data from Bolea-Fernandez et al. (2019)[38] included data of the liver, kidneys, and muscle tissues of juvenile (n = 10, 10, and 8, respectively) and adult (n = 11, 10, and 6, respectively) long-finned pilot whales (*G. melas*). Bolea-Fernandez et al. (2019)[38] also measured $\delta^{202}Hg_t$ in the blood of 7 juvenile and 7 adult pilot whales,

but not *f*(MeHg). The whales were stranded on a Scottish beach in the United Kingdom (September 12, 2012). For liver tissues of Bolea-Fernandez et al. (2019)[38], $[Se]_{tot}$ data were obtained from Gajdosechova et al. (2016).[12] Wet weight $[Hg]_{tot}$ and $[Se]_{tot}$ of Bolea-Fernandez et al. (2019)[38] were converted to dry weight values using the average moisture content of 73.8 ± 2.8% determined by Li et al. (2020) for similar tissues.[36]

Analysis of Hg:Se Ratio: The ratio of Hg to Se was evaluated using the approach outline in Manceau et al. (2021).[6] Briefly, the molar ratio of Hg to Se ($Hg:Se_{chem}$) was determined using chemical measurements. To account for the stoichiometry of the $Hg(Sec)_4$ and HgSe species observed in the whale tissues, the effective Hg:Se ($Hg:Se_{eff}$) was determined (Eq. 2) using values of *f*(HgSe) and *f*($Hg(Sec)_4$) determined by alternating regularization.

$$Hg:Se_{eff} = Hg:Se_{chem} \times (f(HgSe) + 4 \times f(Hg(Sec)_4)) \quad (2)$$

RESULTS AND DISCUSSION

The species distribution of Hg as MeHg, $Hg(Sec)_4$, and HgSe in pilot whale tissues was obtained by calculating iteratively $\delta^{202}Sp_i$ and $f(Sp_{i,t})$ in three steps: (1) an initialization of $\delta^{202}Sp_i$ for each of the three Hg species using the published $\delta^{202}Hg_t$ versus *f*(MeHg) data,[36, 38] (2) an estimation of the fractional amounts of $Hg(Sec)_4$ (*f*($Hg(Sec)_4$)) and HgSe (*f*(HgSe)) using fixed $\delta^{202}Sp_i$ values and measured $\delta^{202}Hg_t$ and *f*(MeHg) values, and (3) an inverse calculation[41] of $\delta^{202}Sp_i$ with fixed *f*($Hg(Sec)_4$) and *f*(HgSe) values and measured $\delta^{202}Hg_t$ and *f*(MeHg) values. Steps 2 and 3 are repeated with new values of *f*($Hg(Sec)_4$), *f*(HgSe), and $\delta^{202}Sp_i$ assigned at every iteration until convergence is reached.

Step 1: Initialization of $\delta^{202}Sp_i$. The Li et al. (2020)[36] and Bolea-Fernandez et al. (2019)[38] data are highly consistent in the trends between bulk $\delta^{202}Hg_t$ and *f*(MeHg) (Fig. 1a,b). $\delta^{202}Hg_t$ values are highest in the muscle and heart tissues with *f*(MeHg) ≈ 1.0 and decrease linearly with decreasing *f*(MeHg) in the muscle, heart, and brain tissues. At *f*(MeHg) ≤ ~0.2, which is observed exclusively in the liver and

kidneys of adult pilot whales, $\delta^{202}Hg_t$ rebounds to more positive values. The ranges of $\delta^{202}Hg_t$ values for the three conditions of *f*(MeHg) are also similar between the two studies: $\delta^{202}Hg_t$ = 1.0 to 1.4‰ for *f*(MeHg) ≈ 1, $\delta^{202}Hg_t$ = -0.4 to 0.3‰ for *f*(MeHg) ≈ 0.0, and $\delta^{202}Hg_t$ exhibits a minimum of ~-1.3‰ at *f*(MeHg) ≈ 0.05 to 0.10. Previous measurements show that MeHg is almost completely demethylated as nanoparticulate HgSe in the liver of pilot whales,[9, 12] and therefore the $\delta^{202}Hg$ value for HgSe was initialized as $\delta^{202}HgSe$ = 0.0‰. One liver tissue of an adult pilot whale from the Li et al. (2020)[36] data is an outlier with $\delta^{202}Hg$ = 0.33‰ for *f*(MeHg) = 0.08 (black arrow in Fig. 1a). Importantly, the hockey stick shape of the $\delta^{202}Hg_t$ versus *f*(MeHg) plots (Fig. 1) suggests the occurrence of an intermediate species in the MeHg → HgSe reaction, which was previously documented to be $Hg(Sec)_4$.[5-7] The analysis here supports that $Hg(Sec)_4$ is highly enriched in lighter Hg isotopes compared to MeHg, consistent with the observed MDF of mercury due to the demethylation of MeHg to $Hg(Sec)_4$,[37] and to a lesser extent HgSe.

Next, initialized $\delta^{202}Hg$ values of MeHg ($\delta^{202}MeHg$) and $Hg(Sec)_4$ ($\delta^{202}Hg(Sec)_4$) were obtained by a linear regression of $\delta^{202}Hg_t$ versus *f*(MeHg) for tissues exempt of HgSe. Fig. 1 shows that the $\delta^{202}Hg_t$ values for muscle, heart, and brain tissues are significantly correlated with *f*(MeHg), and therefore can be used to estimate $\delta^{202}Hg(Sec)_4$. Furthermore, careful study of the data shows that two kidneys of juvenile pilot whales of Li et al. (2020)[36] and several liver and kidneys tissues of Bolea-Fernandez et al. (2019)[38] align with the $\delta^{202}Hg_t$ versus MeHg regression. Therefore, the initial values of $\delta^{202}Hg(Sec)_4$ were determined by regression of the selected tissues of each data set that provided the highest coefficient of determination between $\delta^{202}Hg_t$ versus *f*(MeHg): R^2 = 0.96 for the Li et al. (2020) data (*n* = 23)[36], and R^2 = 0.97 for the Bolea-Fernandez et al. (2019)[38] data (*n* = 35) (Fig. 2 and Tables S1 and S2). The initialized $\delta^{202}Sp_i$ values derived from the two regression lines are $\delta^{202}MeHg$ = 1.26 ± 0.01‰ and $\delta^{202}Hg(Sec)_4$ = -1.56 ± 0.02‰ for the Li et al. (2020) data[36], and $\delta^{202}MeHg$ = 1.20 ± 0.01‰ and $\delta^{202}Hg(Sec)_4$ = -1.33 ± 0.02‰ for the Bolea-Fernandez et al. (2019)[38] data. The regression analyses and

standard deviations (root mean squared error) accounted for the reported uncertainties of both $\delta^{202}Hg_t$ and *f*(MeHg) values. The initialized values of δ^{202}MeHg and $\delta^{202}Hg(Sec)_4$ are remarkably similar in the two studies.

Step 2: Estimation of *f*(Hg(Sec)$_4$) and *f*(HgSe). The measured $\delta^{202}Hg_t$ values in the two pilot whale studies are the weighted averages of the three species-specific δ^{202}MeHg, $\delta^{202}Hg(Sec)_4$, and δ^{202}HgSe values. Therefore, the fractional amounts of $Hg(Sec)_4$ and HgSe in each tissue can be calculated from Equations 3 and 4.

$$(f(\text{MeHg}) \times \delta^{202}\text{MeHg}) + (f(\text{Hg(Sec)}_4) \times \delta^{202}\text{Hg(Sec)}_4) + (f(\text{HgSe}) \times \delta^{202}\text{HgSe}) = \delta^{202}Hg_t \quad (3)$$

$$f(\text{MeHg}) + f(\text{Hg(Sec)}_4) + f(\text{HgSe}) = 1 \quad (4)$$

f(MeHg) is known from chemical measurement. *f*(Hg(Sec)$_4$) and *f*(HgSe) were estimated using the initialized δ^{202}MeHg and $\delta^{202}Hg(Sec)_4$ values obtained from the linear regressions (Fig. 2) and δ^{202}HgSe = 0.00‰ (*Step 1*). The estimated values of *f*(Hg(Sec)$_4$) decreases linearly with increasing *f*(HgSe) in the liver of adult pilot whales in both studies (R^2 = 0.99, Fig. S1a), which is the tissue with the lowest amounts of MeHg. This result confirms that the tissues behave as a ternary system and further supports the interpretation that $Hg(Sec)_4$ is the precursor to nanoparticulate HgSe.[5, 6] *f*(Hg(Sec)$_4$) and *f*(HgSe) also covary negatively in the kidneys of adult pilot whales and in the livers of juveniles (Fig. S1a), but the coefficient of determination between *f*(Hg(Sec)$_4$) and *f*(HgSe) is lower if these tissues are included because they contain more MeHg than the livers of adult whales. The liver tissue of the Li et al. (2020)[36] study that was an outlier (Fig. 1a) is not presented in Figure S1a, as the estimated *f*(Hg(Sec)$_4$) and *f*(HgSe) were outside the feasible range (*f*(Hg(Sec)$_4$) = -0.18, *f*(HgSe) = 1.07).

Step 3: Calculation of $\delta^{202}Sp_i$, *f*(Hg(Sec)$_4$), and *f*(HgSe) by alternating regularized inversion. Eq. 3 can be written in a matrix format

$$\underbrace{\begin{bmatrix} f(\mathrm{MeHg}_1) & f(\mathrm{Hg(Sec)}_{4,1}) & f(\mathrm{HgSe}_1) \\ f(\mathrm{MeHg}_2) & f(\mathrm{Hg(Sec)}_{4,2}) & f(\mathrm{HgSe}_2) \\ \cdots & & \\ f(\mathrm{MeHg}_n) & f(\mathrm{Hg(Sec)}_{4,n}) & f(\mathrm{HgSe}_n) \end{bmatrix}}_{\mathbf{A}} \underbrace{\begin{pmatrix} \delta^{202}\mathrm{MeHg} \\ \delta^{202}\mathrm{Hg(Sec)}_4 \\ \delta^{202}\mathrm{HgSe} \end{pmatrix}}_{\mathbf{x}} = \underbrace{\begin{pmatrix} \delta^{202}\mathrm{Hg}_1 \\ \delta^{202}\mathrm{Hg}_2 \\ .. \\ \delta^{202}\mathrm{Hg}_n \end{pmatrix}}_{\mathbf{b}} \tag{5}$$

where n is the number of tissue samples. Calculating $\delta^{202}\mathrm{Sp}_i$ when $f(\mathrm{Sp}_{i,t})$ and $\delta^{202}\mathrm{Hg}_t$ are known from speciation measurements (e.g., HR-XANES) and isotopic measurements is a well-posed inverse problem.[41] The column vector **x** is obtained by minimizing the misfit functional $\varphi(\mathbf{x})$, or residual, that quantifies the difference between the predicted (**x**) and the observed (**b**) isotopic data

$$\varphi(\mathbf{x}) = \left\| \mathbf{Ax} - \mathbf{b} \right\|^2 = (\mathbf{Ax} - \mathbf{b})^{\mathrm{T}} \mathbf{C}_{\mathrm{d}}^{-1} (\mathbf{Ax} - \mathbf{b}) \tag{6}$$

where $(\mathbf{Ax}\text{-}\mathbf{b})^{\mathrm{T}}$ denotes the transpose of the vector (**Ax**-**b**) and $\mathbf{C}_{\mathrm{d}}^{-1}$ is the inverse matrix of the squared standard deviations of the isotopic measurements. Isotopic measurements are independent and therefore the input covariance $\mathbf{C}_{\mathrm{d}}$ matrix is diagonal and contains the measurement uncertainties of $\delta^{202}\mathrm{Hg}_t$. The unknown vector **x** is obtained at the minimum of the objective functional $\varphi(\mathbf{x})$, which is equivalent to zero its first derivative.

Here, only f(MeHg) and $\delta^{202}\mathrm{Hg}_t$ are known and therefore the problem is ill-posed with non-unique mathematical solutions. Notwithstanding, *a* chemically meaningful solution to $\delta^{202}\mathrm{Sp}_i$ and to the tissue-specific proportions of $\mathrm{Hg(Sec)}_4$ and HgSe can be obtained simultaneously by an alternating regularized inversion method.[40] The approach necessitates addition of a regularization term to the objective function.

$$\varphi(\mathbf{x}) = \left\| \mathbf{Ax} - \mathbf{b} \right\|^2 = (\mathbf{Ax} - \mathbf{b})^{\mathrm{T}} \mathbf{C}_{\mathrm{d}}^{-1} (\mathbf{Ax} - \mathbf{b}) + \lambda \mathbf{x}^{\mathrm{T}} \mathbf{x} \tag{7}$$

The regularization term $\mathbf{x}^{\mathrm{T}}\mathbf{x}$ allows one to penalize large (i.e., meaningless) values in **x** and is weighted by the user-defined λ parameter. The weighting parameter λ was determined using the so-called *L-curve criterion* defined as

$$\lambda = 0.01 \times \max\left(\mathbf{A}^{\mathrm{T}}\mathbf{C}_{\mathrm{d}}^{-1}\mathbf{A}\right) \tag{8}$$

for both the Li et al. (2020)[36] and the Bolea-Fernandez et al. (2019)[38] data sets, which is a reasonable value for inverse problems.[42] Using the notation in Eq. 7, the optimal **x** value, as obtained by zeroing the first derivative of the objective function, is

$$\mathbf{x} = [\mathbf{A}^{\mathrm{T}}\mathbf{C}_{\mathrm{d}}^{-1}\mathbf{A} + \lambda\mathbf{I}]^{-1}\mathbf{A}^{\mathrm{T}}\mathbf{C}_{\mathrm{d}}^{-1}\mathbf{b} \tag{9}$$

where **I** is the identity matrix.

The workflow schematic for the inversion calculations is presented in Fig. 3. First, the inversion scheme starts with an *a priori* estimate of $\delta^{202}Sp_i$ (initialization *Step* 1 described above), in which δ^{202}MeHg and $\delta^{202}Hg(Sec)_4$ are the values obtained from the $\delta^{202}Hg_t$ versus *f*(MeHg) regression (Fig. 2) and δ^{202}HgSe is set to 0‰. Second, a two-step alternating reconstruction is performed, in which *f*($Hg(Sec)_4$) and *f*(HgSe) are obtained from Eq. 3 and 4 using the preset $\delta^{202}Sp_i$ values (*Step* 2), and $\delta^{202}Sp_i$ is calculated next from Eq. 9 using the previously calculated *f*($Hg(Sec)_4$) and *f*(HgSe) values (*Step* 3). The two variable sets are updated alternatively at each step of the leap-frog process until $\varphi(\mathbf{x})$ converges to a minimum.

The linear system in *Step 2* is well-posed and always provides a unique solution. However, *f*($Hg(Sec)_4$) and *f*(HgSe) may be negative or >1 if the *a priori* $\delta^{202}Sp_i$ values are unrealistic. When this is the case, the algorithm automatically projects the unacceptable fractions onto a user-defined admissible range. In the pilot whale data analyzed here, it was observed that a small negative value of *f*($Hg(Sec)_4$) and *f*(HgSe) equal to the uncertainty of the known *f*(MeHg) value (e.g., ± 0.05) did not prevent global convergence. The number of iterations in the inner loop increased from 513 to 533 for the Li et al. (2020) data,[36] and from 231 to 237 for the Bolea-Fernandez et al. (2019) data,[38] when the criterion of the upper and lower limits for *f*($Hg(Sec)_4$) and *f*(HgSe) was changed from ± 0.01 to ± 0.05, but the optimal $\delta^{202}Sp_i$, *f*($Hg(Sec)_4$), and *f*(HgSe) values were identical with the two criteria. The

reliability of the iterative method was also evaluated by varying the initial estimate of δ^{202}HgSe. The reconstruction algorithm converged to the same solution when the initial δ^{202}HgSe values for the Li et al. (2020)[36] and the Bolea-Fernandez et al. (2019)[38] data sets were set to the experimental value of the liver tissue containing the lowest proportion of MeHg (f(MeHg) = 0.043, δ^{202}HgSe = -0.32‰ and f(MeHg) = 0.009, δ^{202}HgSe = -0.35‰, respectively, Tables S1 and S2).

The optimal solutions are δ^{202}MeHg = 1.23‰, δ^{202}Hg(Sec)$_4$ = -1.46‰, δ^{202}HgSe = 0.00‰ for the Li et al. (2020)[36] data, and δ^{202}MeHg = 1.17‰, δ^{202}Hg(Sec)$_4$ = -1.29‰, δ^{202}HgSe = 0.00‰ for the Bolea-Fernandez et al. (2019)[38] data. The δ^{202}MeHg and δ^{202}Hg(Sec)$_4$ values are in good agreement with those derived from the regression analysis in the initialization step; 1.26‰ and 1.20‰ for δ^{202}MeHg and -1.56‰ and -1.33‰ for δ^{202}Hg(Sec)$_4$ for the Li et al. (2020)[36] data and Bolea-Fernandez et al. (2019)[38] data, respectively. The alternating inversion method quantifies δ^{202}HgSe, whereas the δ^{202}Hg$_t$ versus f(MeHg) analysis (*Step 1*) only provides an estimate of δ^{202}HgSe. Formal uncertainties cannot be calculated on species-specific δ^{202}Hg values because the alternating inversion scheme is in essence nonlinear and due to the regularization term ($\lambda \mathbf{x}^T x$). To estimate accuracy of the alternating inversion method, the δ^{202}Sp$_i$ values were calculated using the two independent data sets together (n = 89) and compared with the results presented above on each data set. Analyzed together, the δ^{202}Sp$_i$ values (δ^{202}MeHg = 1.21‰, δ^{202}Hg(Sec)$_4$ = -1.37‰, and δ^{202}HgSe = 0.00‰) quantify that the uncertainty in the calculated δ^{202}Sp$_i$ values is < 0.1‰.

Proportions of the Hg species in pilot whale tissues. The proportions of MeHg, Hg(Sec)$_4$, and HgSe (f(Sp$_i$)) in long-finned pilot whale tissues of Li et al. (2020)[36] (n = 34) and Bolea-Fernandez et al. (2019)[38] (n = 55) are reported in Tables S1 and S2 and presented graphically in Figure 4. The sum of the proportions of Hg species being normalized to 1 (Eq. 4), the f(Sp$_i$) values define a hyperplane within the three-dimensional f(MeHg), f(Hg(Sec)$_4$), f(HgSe) space. The f(Sp$_i$) values are distributed in the hyperplane within an equilateral triangle with one Hg species at each vertice. The two triangles obtained

with the Li et al. (2020)[36] and the Bolea-Fernandez et al. (2019)[38] data sets are represented in a three-dimensional space in Figure 4a with $\delta^{202}Hg_t$ as the third dimension. The two triangles are practically superimposed in this space, which confirms the high consistency between the two independent data sets.

A two-dimensional projection of the two $f(Sp_i)$ ternary diagrams is shown in Figure 4b. Tissues of the pilot whales organize into three classes based on mercury species distribution. First, in the heart and muscle tissues of juvenile and adult whales, mercury is primarily present as MeHg with a low fraction as $Hg(Sec)_4$ and no HgSe. Second, in the brain of both juvenile and adult whales and most juvenile kidneys tissues, mercury is present as a mixture of MeHg and $Hg(Sec)_4$. Third, in adult kidneys and both juvenile and adult liver tissues, mercury is present as minor MeHg and a mixture of both $Hg(Sec)_4$ and HgSe. When evaluated in context of the total concentration of mercury ($[Hg]_{tot}$) in tissues, the fluctuations in $f(Sp_i)$ with increasing $[Hg]_{tot}$ document the step-wise MeHg → $Hg(Sec)_4$ → HgSe demethylation reaction (Fig. 5a-5c). f(MeHg) decreases and f(HgSe) increases with the extent of the reaction, which progresses with $[Hg]_{tot}$, and $f(Hg(Sec)_4)$ exhibits a unimodal behavior reflecting the intermediate species of the reaction. $f(Hg(Sec)_4)$ and f(HgSe) covary negatively (Fig. S1b), similar to the observed trend between estimates of $f(Hg(Sec)_4)$ and f(HgSe) from the initialization step (*Step 1*, Fig. S1a). The correlation between $f(Hg(Sec)_4)$ and f(HgSe) reflects the biomineralization of nanoparticulate HgSe from precursor $Hg(Sec)_4$.[5, 6] Further, the ratios of $f(Sp_i)$ values for the MeHg → $Hg(Sec)_4$ reaction ($f(Hg(Sec)_4)/f$(MeHg)) and $Hg(Sec)_4$ → HgSe reaction (f(HgSe)/$f(Hg(Sec)_4)$) are diagnostic of the extent of the two step reaction (Fig. 5d and 5e). Across all tissues, $f(Hg(Sec)_4)/f$(MeHg) is greater in adult compared to juvenile whales for a given tissue and exhibit a hierarchy of heart < muscle < brain < kidneys < liver (Fig. 5d). Similarly, of the tissues with HgSe, f(HgSe)/$f(Hg(Sec)_4)$ is greater in adult compared to juvenile whales and liver compared to kidneys tissues (Fig. 5e).

The weight concentrations of the three Hg species are obtained by multiplying $f(Sp_i)$ by $[Hg]_{tot}$ and are presented in Figure 6 for each tissue in ascending order of $[Hg]_{tot}$. Trends in weighted concentrations

of the three Hg species highlight two notable observations. First, the high abundance of $Hg(Sec)_4$ in the brain of juvenile and adult whales, compared to the muscle and heart of similar $[Hg]_{tot}$ (Fig. 6a-c), suggests that the brain is better protected against Hg toxicity than muscular tissues. An evaluation of the ratio of Hg to Se ($Hg:Se_{eff}$), accounting for the stoichiometric ratio of $Hg(Sec)_4$ (1:4),[6] indicates that the demethylation of MeHg in the adult whale brain could deplete bioavailable reservoirs of Se ($1.1 < Hg:Se_{eff} < 3.1$) (Tables S1 and S2). It is likely, however, that the brains of adult whales contain polynuclear $Hg_x(Se,Sec)_y$ clusters rather than strict mononuclear $Hg(Sec)_4$ complexes, the former observed in waterbird[5] and seabird[6] and understood to represent an intermediate in the biomineralization of HgSe from $Hg(Sec)_4$. $Hg_x(Se,Sec)_y$ clusters have $1 < Hg:Se < 4$, therefore omitting this species in the estimation of $Hg:Se_{eff}$ underestimates the amount of bioavailable Se.[6] The possible neurotoxic effects of Se deficiency due to MeHg demethylation require further study. Second, the primary locations for the detoxification of MeHg are the liver, kidneys, and brain, and the accumulation of demethylated species ($Hg(Sec)_4$ and HgSe) account for Hg burden in these tissues (Fig. 6). In the kidneys and liver of whales, where the MeHg → $Hg(Sec)_4$ → HgSe demethylation reaction is most advanced, there is no apparent threshold Hg concentration above which the demethylation of MeHg into $Hg(Sec)_4$ and HgSe is initiated. In contrast, a demethylation threshold of approximately 8.5 mg Hg/kg dry weight (dw) has been reported in the liver of waterbirds.[43] This may reflect the greater availability of selenium in marine systems that yield efficient MeHg → $Hg(Sec)_4$ demethylation across broad tissues.[36, 38]

To put into context the Hg speciation results in long-finned pilot whales, a diagrammatic picture of the average concentrations and speciation of Hg in the tissues of whales juveniles and adults (Fig. S2a,b) are compared to those obtained recently in giant petrel (*Macronectes* spp) using HR-XANES (Fig. S2c).[6] Petrels are top predator of food webs and scavengers of mammal and bird carcasses, and therefore contain similar amounts of mercury as long-finned pilot whales. In petrel, HgSe occurs not only in liver and kidneys, but also in brain and muscle. Almost all the Hg is in the form of HgSe in liver, and the

brain contains 38 ± 32% HgSe, despite having less Hg (5.9 ± 6.4 mg/kg dw) than the whales brains from the Li et al.(2020)[36] study (13.8 ± 7.9 mg/kg dw). Overall, petrels seem to detoxify MeHg more efficiently than long-finned pilot whales, for reasons yet to be known, making life apparently more compatible with such high contaminant burden.

CONCLUDING REMARKS

We demonstrated that the atomic-level biochemistry of toxic methylmercury (MeHg) and its degradation products in biological tissues can be obtained by a mathematical treatment of the Hg isotope data using an iterative regularization method. Inversion methods are used in many fields of science,[41, 44] but this is the first application with stable isotopic data. The algorithm, which we developed, was used to probe the internal transformations of mercury in the liver, kidneys, muscle, heart, and brain of long-finned pilot whales. We showed that the hockey stick shape of the $\delta^{202}Hg_t$ versus f(MeHg) graph of whale tissues reflects the step-wise MeHg → $Hg(Sec)_4$ → HgSe reaction and metabolic processes leading to a change of Hg speciation in and across tissues. The isotopic data can be explained by the coexistence of MeHg with two inorganic species, $Hg(Sec)_4$ and HgSe, with uniform isotopic signatures: δ^{202}MeHg = 1.21 ± 0.04‰, $\delta^{202}Hg(Sec)_4$ = -1.37 ± 0.09‰, and δ^{202}HgSe = 0.00 ± 0.00‰. The $\delta^{202}Hg(Sec)_4$ - δ^{202}MeHg difference of 2.58 ± 0.13‰ is similar to that reported recently for birds (-2.2 ± 0.1‰).[37]

A highlight of this study is the invariance of the three $\delta^{202}Sp_i$ values between the tissues of a same individual, across individuals of the same pod, and between pods sampled at different times in different geographic locations. A similar observation was made previously for the uniformity of δ^{202}Hg in the blood of 7 juvenile and 7 adult whales ($\delta^{202}Hg_{blood}$ = 1.06 ± 0.05‰).[38] Li et al. (2020)[36] interpreted the blood results and the linear relationship of δ^{202}Hg with f(MeHg) in the heart, brain, and muscle of whales (Fig. 1a,b) to indicate that the isotopic composition of MeHg is constantly homogenized throughout the

body. The isotopic equilibrium of MeHg reported here agrees with the rapid shifts in Hg isotope values of fish tissues to values of dietary MeHg.[45]

We explain the steady state isotopic fractionation of $Hg(Sec)_4$ and HgSe by (1) a continuous input of isotopically constant MeHg source from the diet, (2) continuous exchange of MeHg and $Hg(Sec)_4$ between the circulatory system and tissues, and (3) the rapid turnover of Hg-carrying proteins and elimination of Hg in urine and feces. The circulation of $Hg(Sec)_4$ in whale blood is supported experimentally by the analysis of Se-containing proteins in the plasma of Inuits, which showed that up to 50% of Hg is associated with SelP.[46] Blood isotopic analysis offers suggestive evidence for the presence of $Hg(Sec)_4$ in the circulatory system. In whales studied by Bolea-Fernandez et al. (2019),[38] $\delta^{202}Hg_{blood}$ = 1.06 ± 0.05‰ while δ^{202}MeHg obtained in all tissues by the alternating regularized inversion is 1.17‰. The circulation of $Hg(Sec)_4$ in the blood at 4% of the total Hg concentration could account for the 0.11‰ difference observed between the $\delta^{202}Hg_{blood}$ and δ^{202}MeHg. In conclusion, this study establishes the possibility to probe the atomic-level chemistry of mercury in animal tissues from species-averaged isotopic data and *f*(MeHg) alone, without complementary structural information from HR-XANES spectroscopy. This approach will facilitate advancement of the next generation of toxicokinetic models for mercury across diverse organisms.

ASSOCIATED CONTENT

Supporting Information

The Supporting Information is available free of charge on the ACS Publications website at DOI:

Supplementary table and figures (PDF)

AUTHOR INFORMATION

Corresponding Author

E-mail: alain.manceau@univ-grenoble-alpes.fr

ORCID

Alain Manceau: 0000-0003-0845-611X

Romain Brossier: 0000-0002-7195-8123

Brett A. Poulin: 0000-0002-5555-7733

Notes

The authors declare no competing financial interests.

ACKNOWLEDGMENTS

Financial support was provided to Brett A. Poulin by the U.S. National Science Foundation under grant EAR-1629698.

REFERENCES

(1) Douglas, T. A.; Loseto, L. L.; Macdonald, R. W.; Outridge, P.; Dommergue, A.; Poulain, A.; Amyot, M.; Barkay, T.; Berg, T.; Chetelat, J.; Constant, P.; Evans, M.; Ferrari, C.; Gantner, N.; Johnson, M. S.; Kirk, J.; Kroer, N.; Larose, C.; Lean, D.; Nielsen, T. G.; Poissant, L.; Rognerud, S.; Skov, H.; Sorensen, S.; Wang, F. Y.; Wilson, S.; Zdanowicz, C. M. The fate of mercury in Arctic terrestrial and aquatic ecosystems, a review. *Environmental Chemistry* **2012,** *9*, 321-355.

(2) Driscoll, C. T.; Mason, R. P.; Chan, H. M.; Jacob, D. J.; Pirrone, N. Mercury as a global pollutant: Sources, pathways, and effects. *Env. Sci. Technol.* **2013,** *47*, 4967-4983.

(3) Lehnherr, I. Methylmercury biogeochemistry: a review with special reference to Arctic aquatic ecosystems. *Environ. Rev.* **2014,** *22*, 229-243.

(4) Eagles-Smith, C. A.; Silbergeld, E. K.; Basu, N.; Bustamante, P.; Diaz-Barriga, F.; Hopkins, W. A.; Kidd, K. A.; Nyland, J. F. Modulators of mercury risk to wildlife and humans in the context of rapid global change. *Ambio* **2018,** *47*, 170-197.

(5) Manceau, A.; Bourdineaud, J. P.; Oliveira, R. B.; Sarrazin, S. L. F.; Krabbenhoft, D. P.; Eagles-Smith, C. A.; Ackerman, J. T.; Stewart, A. R.; Ward-Deitrich, C.; Busto, M. E. D.; Goenaga-Infante, H.; Wack, A.; Retegan, M.; Detlefs, B.; Glatzel, P.; Bustamante, P.; Nagy, K. L.; Poulin, B. A. Demethylation of methylmercury in bird, fish, and earthworm. *Environ. Sci. Technol.* **2021,** *55*, 1527-1534.

(6) Manceau, A.; Gaillot, A. C.; Glatzel, P.; Cherel, Y.; Bustamante, P. In vivo formation of HgSe nanoparticles and Hg-tetraselenolate complex from methylmercury in seabird – Implications for the Hg-Se antagonism. *Environ. Sci. Technol.* **2021,** *55*, 1515-1526.

(7) Manceau, A.; Azemard, S.; Hédouin, L.; Vassileva, E.; Lecchini, D.; Fauvelot, C.; Swarzenski, P. W.; Glatzel, P.; Bustamante, P.; Metian, M. The chemical forms of mercury in blue marlin billfish: Implications for human exposure. *Environ. Sci.. Technol. Lett.* **2021**, https://pubs.acs.org/doi/10.1021/acs.estlett.1c00217.

(8) Arai, T.; Ikemoto, T.; Hokura, A.; Terada, Y.; Kunito, T.; Tanabe, S.; Nakai, I. Chemical forms of mercury and cadmium accumulated in marine mammals and seabirds as determined by XAFS analysis. *Environ. Sci. Technol.* **2004,** *38*, 6468-6474.

(9) Nakazawa, E.; Ikemoto, T.; Hokura, A.; Terada, Y.; Kunito, T.; Tanabe, S.; Nakai, I. The presence of mercury selenide in various tissues of the striped dolphin: evidence from μ-XRF-XRD and XAFS analyses. *Metallomics* **2011,** *3*, 719-725.

(10) Lailson-Brito, J.; Cruz, R.; Dorneles, P. R.; Andrade, L.; Azevedo, A. D.; Fragoso, A. B.; Vidal, L. G.; Costa, M. B.; Bisi, T. L.; Almeida, R.; Carvalho, D. P.; Bastos, W. R.; Malm, O. Mercury-selenium relationships in liver of Guiana dolphin: The possible role of Kupffer cells in the detoxification process by tiemannite formation. *Plos One* **2012,** *7*, n° e42162.

(11) Sakamoto, M.; Itai, T.; Yasutake, A.; Iwasaki, T.; Yasunaga, G.; Fujise, Y.; Nakamura, M.; Murata, K.; Chan, H. M.; Domingo, J. L.; Marumoto, M. Mercury speciation and selenium in toothed-whale muscles. *Environ. Res.* **2015,** *143*, 55-61.

(12) Gajdosechova, Z.; Lawan, M. M.; Urgast, D. S.; Raab, A.; Scheckel, K. G.; Lombi, E.; Kopittke, P. M.; Loeschner, K.; Larsen, E. H.; Woods, G.; Brownlow, A.; Read, F. L.; Feldmann, J.; Krupp, E. M. In vivo formation of natural HgSe nanoparticles in the liver and brain of pilot whales. *Sci. Rep.* **2016,** *6*, 34361.

(13) Harris, H. H.; Pickering, I. J.; George, G. N. The chemical form of mercury in fish. *Science* **2003,** *301*, 1203.

(14) Kuwabara, J. S.; Arai, Y.; Topping, B. R.; Pickering, I. J.; George, G. N. Mercury speciation in piscivorous fish from mining-impacted reservoirs. *Environ. Sci. Technol.* **2007,** *41*, 2745-2749.

(15) Huggins, F. E.; Raverty, S. A.; Nielsen, O. S.; Sharp, N. E.; Robertson, J. D.; Ralston, N. V. C. An XAFS investigation of mercury and selenium in Beluga whale tissues. *Environ. Bioindic.* **2009,** *4*, 291-302.

(16) George, G. N.; MacDonald, T. C.; Korbas, M.; Singh, S. P.; Myers, G. J.; Watson, G. E.; O'Donoghue, J. L.; Pickering, I. J. The chemical forms of mercury and selenium in whale skeletal muscle. *Metallomics* **2011,** *3*, 1232-1237.

(17) Korbas, M.; O'Donoghue, J. L.; Watson, G. E.; Pickering, I. J.; Singh, S. P.; Myers, G. J.; Clarkson, T. W.; George, G. N. The chemical nature of mercury in human brain following poisoning or environmental exposure. *ACS Chem. Neurosci.* **2010,** *1*, 810-818.

(18) MacDonald, T. C.; Korbas, M.; James, A. K.; Sylvain, N. J.; Hackett, M. J.; Nehzati, S.; Krone, P. H.; George, G. N.; Pickering, I. J. Interaction of mercury and selenium in the larval stage zebrafish vertebrate model. *Metallomics* **2015,** *7*, 1247-1255.

(19) Manceau, A.; Enescu, M.; Simionovici, A.; Lanson, M.; Gonzalez-Rey, M.; Rovezzi, M.; Tucoulou, R.; Glatzel, P.; Nagy, K. L.; Bourdineaud, J.-P. Chemical forms of mercury in human hair reveal sources of exposure. *Environ. Sci. Technol.* **2016,** *50*, 10721–10729.

(20) Thomas, S. A.; Gaillard, J. F. Cysteine addition promotes sulfide production and four-fold Hg(II)-S coordination in actively metabolizing *Escherichia coli*. *Environ. Sci. Technol.* **2017,** *51*, 4642-4651.

(21) Thomas, S. A.; Rodby, K. E.; Roth, E. W.; Wu, J.; Gaillard, J. F. Spectroscopic and microscopic evidence of biomediated HgS species formation from Hg(II)–cysteine complexes: Implications for Hg(II) bioavailability. *Environ. Sci. Technol.* **2018,** *52*, 10030-10039.

(22) Thomas, S. A.; Mishra, B.; Myneni, S. C. B. Cellular mercury coordination environment, and not cell surface ligands, influence bacterial methylmercury production. *Environ. Sci. Technol.* **2020,** *54*, 3960-3968.

(23) Pickering, I. J.; Cheng, Q.; Rengifo, E. M.; Nehzati, S.; Dolgova, N. V.; Kroll, T.; Sokaras, D.; George, G. N.; Arner, E. S. J. Direct observation of methylmercury and auranofin binding to selenocysteine in thioredoxin reductase. *Inorg Chem.* **2020,** *59*, 2711-2718.

(24) Bourdineaud, J. P.; Durn, G.; Režun, B.; Manceau, A.; Hrenović, J. The chemical species of mercury accumulated by *Pseudomonas idrijaensis*, a bacterium from a rock of the Idrija mercury mine, Slovenia. *Chemosphere* **2020,** *248*, n° 126002.

(25) Minet, A.; Manceau, A.; Valada-Mennuni, A.; Brault-Favrou, M.; Churlaud, C.; Fort, J.; Nguyen, T. C.; Spitz, J.; Bustamante, P.; Lacoue-Labarthe, T. Mercury in the tissues of five cephalopods species: first data on the nervous system *Sci. Tot. Environ.* **2021,** *759*, n° 143907.

(26) Manceau, A.; Nagy, K. L.; Glatzel, P.; Bourdineaud, J. P. Acute toxicity of divalent mercury to bacteria explained by the formation of dicysteinate and tetracysteinate complexes bound to proteins in *Escherichia coli* and *Bacillus subtilis*. *Environ. Sci. Technol.* **2021,** *55*, 3612-3623.

(27) Eiler, J. M.; Bergquist, B.; Bourg, I.; Cartigny, P.; Farquhar, J.; Gagnon, A.; Guo, W. F.; Halevy, I.; Hofmann, A.; Larson, T. E.; Levin, N.; Schauble, E. A.; Stolper, D. Frontiers of stable isotope geoscience. *Chem. Geol.* **2014,** *372*, 119-143.

(28) Sherman, L. S.; Blum, J. D.; Franzblau, A.; Basu, N. New insight into biomarkers of human mercury exposure using naturally occurring mercury stable isotopes. *Environ. Sci. Technol.* **2013,** *47*, 3403-3409.

(29) Li, M. L.; Sherman, L. S.; Blum, J. D.; Grandjean, P.; Mikkelsen, B.; Weihe, P.; Sunderland, E. M.; Shine, J. P. Assessing sources of human methylmercury exposure using stable mercury isotopes. *Environ. Sci. Technol.* **2014,** *48*, 8800-8806.

(30) Blum, J. D.; Sherman, L. S.; Johnson, M. W. Mercury isotopes in Earth and environmental sciences. In *Annu. Rev. Earth Planet. Sci.*, Jeanloz, R., Ed. 2014; Vol. 42, pp 249-269.

(31) Wiederhold, J. G. Metal stable isotope signatures as tracers in environmental geochemistry. *Environ. Sci. Technol.* **2015**, 2606-2624.

(32) Renedo, M.; Amouroux, D.; Duval, B.; Carravieri, A.; Tessier, E.; Barre, J.; Berail, S.; Pedrero, Z.; Cherel, Y.; Bustamante, P. Seabird tissues as efficient biomonitoring tools for Hg isotopic investigations: Implications of using blood and feathers from chicks and adults. *Environ. Sci. Technol.* **2018,** *52*, 4227-4234.

(33) Renedo, M.; Pedrero, Z.; Amouroux, D.; Cherel, Y.; Bustamante, P. Mercury isotopes of key tissues document mercury metabolic processes in seabirds. *Chemosphere* **2021,** *263*, n° 127777.

(34) Tsui, M. T. K.; Blum, J. D.; Kwon, S. Y. Review of stable mercury isotopes in ecology and biogeochemistry. *Sci. Tot. Environ.* **2020,** *716*.

(35) Perrot, V.; Masbou, J.; Pastukhov, M. V.; Epov, V. N.; Point, D.; Berail, S.; Becker, P. R.; Sonke, J. E.; Amouroux, D. Natural Hg isotopic composition of different Hg compounds in mammal tissues as a proxy for in vivo breakdown of toxic methylmercury. *Metallomics* **2016,** *8*, 170-178.

(36) Li, M. L.; Juang, C. A.; Ewald, J. D.; Yin, R. S.; Mikkelsen, B.; Krabbenhoft, D. P.; Balcom, P. H.; Dassuncao, C.; Sunderland, E. M. Selenium and stable mercury isotopes provide new insights into mercury toxicokinetics in pilot whales. *Sci. Tot. Environ.* **2020,** *710*, n° 136325.

(37) Poulin, B. A.; Janssen, S. E.; Rosera, T. J.; Krabbenhoft, D. P.; Eagles-Smith, C. A.; Ackerman, J. T.; Stewart, A. R.; Kim, E.; Baumann, Z.; Kim, J. H.; Manceau, A. Isotope fractionation from *in vivo* methylmercury detoxification in waterbirds. *ACS Earth Space Chem.* **2021**, https://pubs.acs.org/doi/10.1021/acsearthspacechem.1c00051.

(38) Bolea-Fernandez, E.; Rua-Ibarz, A.; Krupp, E. M.; Feldmann, J.; Kvanhaecke, F. High-precision isotopic analysis sheds new light on mercury metabolism in long-finned pilot whales (*Globicephala melas*). *Sci. Reports* **2019,** *9*, n° 7262.

(39) Virieux, J.; Operto, S. An overview of full-waveform inversion in exploration geophysics. *Geophysics* **2009,** *74*, WCC1-WCC26.

(40) Rizzuti, G.; Gisolf, A. An iterative method for 2D inverse scattering problems by alternating reconstruction of medium properties and wavefields: theory and application to the inversion of elastic waveforms. *Inverse Probl.* **2017,** *33*.

(41) Tarantola, A. *Inverse Problem Theory and Methods for Model Parameter Estimation*. Society for Industrial and Applied Mathematics, Philadelphia: 2005; p 342.

(42) Calvetti, D.; Morigi, S.; Reichel, L.; Sgallari, F. Tikhonov regularization and the L-curve for large discrete ill-posed problems. *J. Comput. Appl. Math.* **2000,** *123*, 423-446.

(43) Eagles-Smith, C. A.; Ackerman, J. T.; Yee, J.; Adelsbach, T. L. mercury demethylation in waterbird livers: dose-response thresholds and differences among species. *Environ. Toxicol. Chem.* **2009,** *28*, 568-577.

(44) Kaipio, J.; Somersalo, E. *Statistical and computational inverse problems.* . Springer.: New York, NY, 2010.

(45) Kwon, S. Y.; Blum, J. D.; Chirby, M. A.; Chesney, E. J. Application of mercury isotopes for tracing trophic transfer and internal distribution of mercury in marine fish feeding experiments. *Environ. Toxicol. Chem.* **2013,** *32*, 2322-2330.

(46) Achouba, A.; Dumas, P.; Ouellet, N.; Lemire, M.; Ayotte, P. Plasma levels of selenium-containing proteins in Inuit adults from Nunavik. *Environ. Intern.* **2016,** *96*, 8-15.

FIGURE CAPTION

Fig. 1. Relationship between δ^{202}Hg and *f*(MeHg) in long-finned pilot whales tissues. (a) Li et al. (2020)[36] data. (b) Bolea-Fernandez et al. (2019)[38] data. Filled and open data points are tissues from adult (A) and juvenile (J) pilot whales, respectively. Error bars present the associated error of measured δ^{202}Hg. In plot (a) the arrow identifies an outlier.

Fig. 2. Selection of long-finned pilot whales tissues giving the best linear regression between δ^{202}Hg and *f*(MeHg). (a) Li et al. (2020)[36] data. $\delta^{202}Hg = -1.56 + 2.82 \times f(MeHg)$ ($R^2 = 0.96$). (b) Bolea-Fernandez et al. (2019)[38] data. $\delta^{202}Hg = -1.33 + 2.53 \times f(MeHg)$ ($R^2 = 0.97$). Filled and open data points are tissues from adult (A) and juvenile (J) pilot whales, respectively. Error bars present the associated error of measured δ^{202}Hg.

Fig. 3. Workflow of the alternating regularized inversion algorithm used to calculate $^{202}Sp_i$ from $^{202}Hg_t$ and *f*(MeHg). Step 1: initialization of $\delta^{202}Sp_i$ from the $\delta^{202}Hg_t$ versus *f*(MeHg) data. Step 2: regression analysis of $f(Hg(Sec)_4)$ and *f*(HgSe) with fixed $\delta^{202}Sp_i$ values. Step 3: inversed calculation[41] of $\delta^{202}Sp_i$ with fixed $f(Hg(Sec)_4)$ and *f*(HgSe) values. Steps 2 and 3 are repeated with $f(Hg(Sec)_4)$, *f*(HgSe), $\delta^{202}Sp_i$ re-assigned new values at every iteration until convergence is reached.

Fig. 4. Proportions of the three Hg species ($f(Sp_i)$) in tissues of long-finned pilot whales as calculated with the alternating regularized inversion method. (a) Three-dimensional view of the ternary planes defined given by f(MeHg), $f(Hg(Sec)_4)$, and f(HgSe) with $\delta^{202}Hg_t$ as the third dimension. Cyan color refers to the Li et al. (2020)[36] data set and magenta color refers to the Bolea-Fernandez et al. (2019)[38] data set. (b) Two-dimensional projection of the two ternary planes.

Fig. 5. Proportions of the three Hg species (a) f(MeHg), (b) $f(Hg(Sec)_4)$, (c) f(HgSe)) as a function of the total Hg concentration ($[Hg]_{tot}$). Box plots of median and quartile ranges of the ratio of (d) $f(Hg(Sec)_4)$ to f(MeHg) and (e) f(HgSe) to $f(HgSec)_4$ for juvenile (open) and adult (filled) whale tissues. In plots (d) and €, error bars represent 10% and 90% percentiles and outliers are shown as data points.

Fig. 6. Stacked bar charts of the concentrations (dry weight, dw) of the three Hg species (Sp_i) in the heart (a), muscle (b), brain (c), kidneys (d), and liver (e) of long-finned pilot whales. Concentrations were determined using the proportions of Hg species ($f(Sp_i)$) determined by the alternating regularized inversion method and total Hg concentration published in Li et al. (2020)[36] and Bolea-Fernandez et al. (2019).[38] In each sub-plot, tissues are presented in ascending order of total Hg concentration and the vertical dashed line identifies the separation between juvenile and adult whales. The asterisk in plot d indicates a juvenile whale.

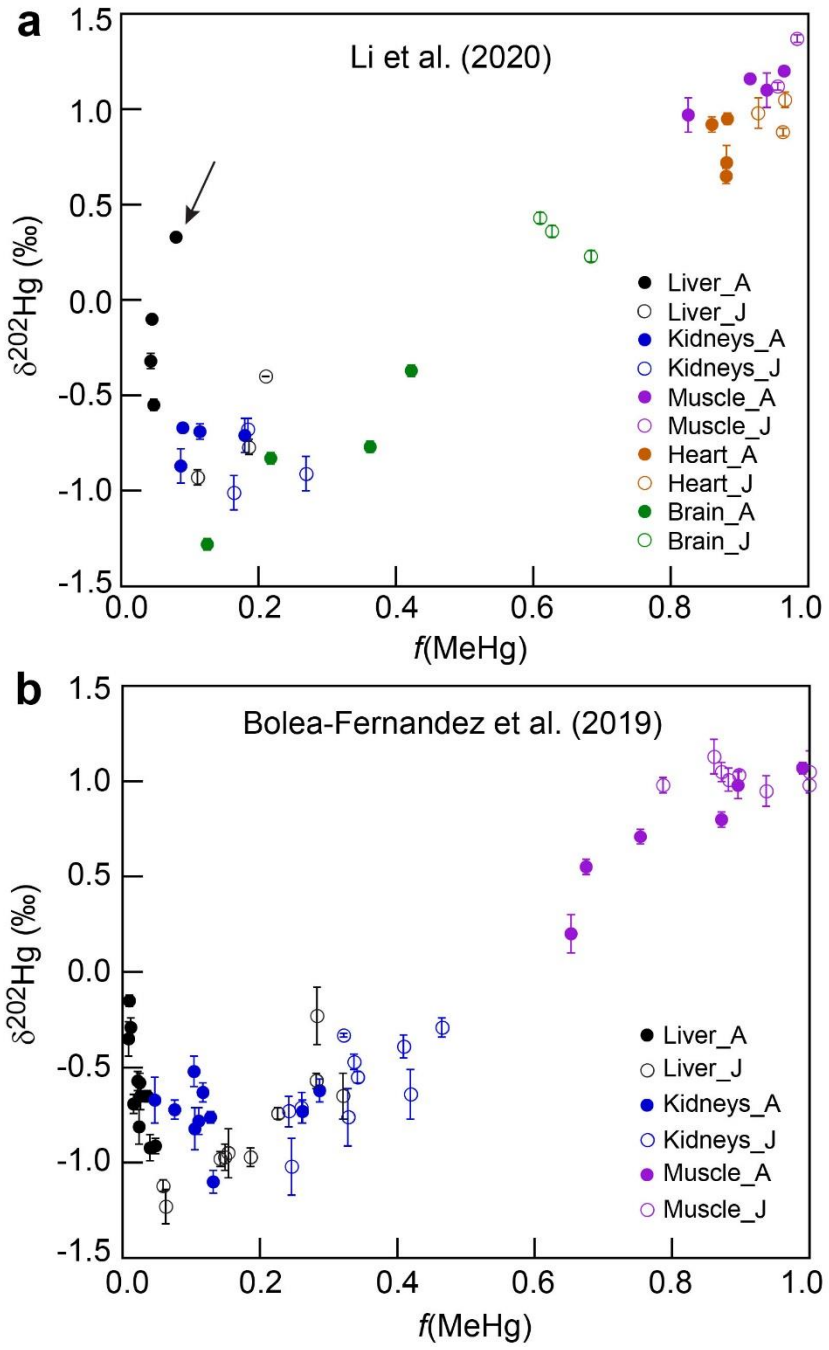
a
Li et al. (2020)
δ202Hg (‰)
f(MeHg)
Liver_A
Liver_J
Kidneys_A
Kidneys_J
Muscle_A
Muscle_J
Heart_A
Heart_J
Brain_A
Brain_J
b
Bolea-Fernandez et al. (2019)
δ202Hg (‰)
f(MeHg)
Liver_A
Liver_J
Kidneys_A
Kidneys_J
Muscle_A
Muscle_J

Figure 1

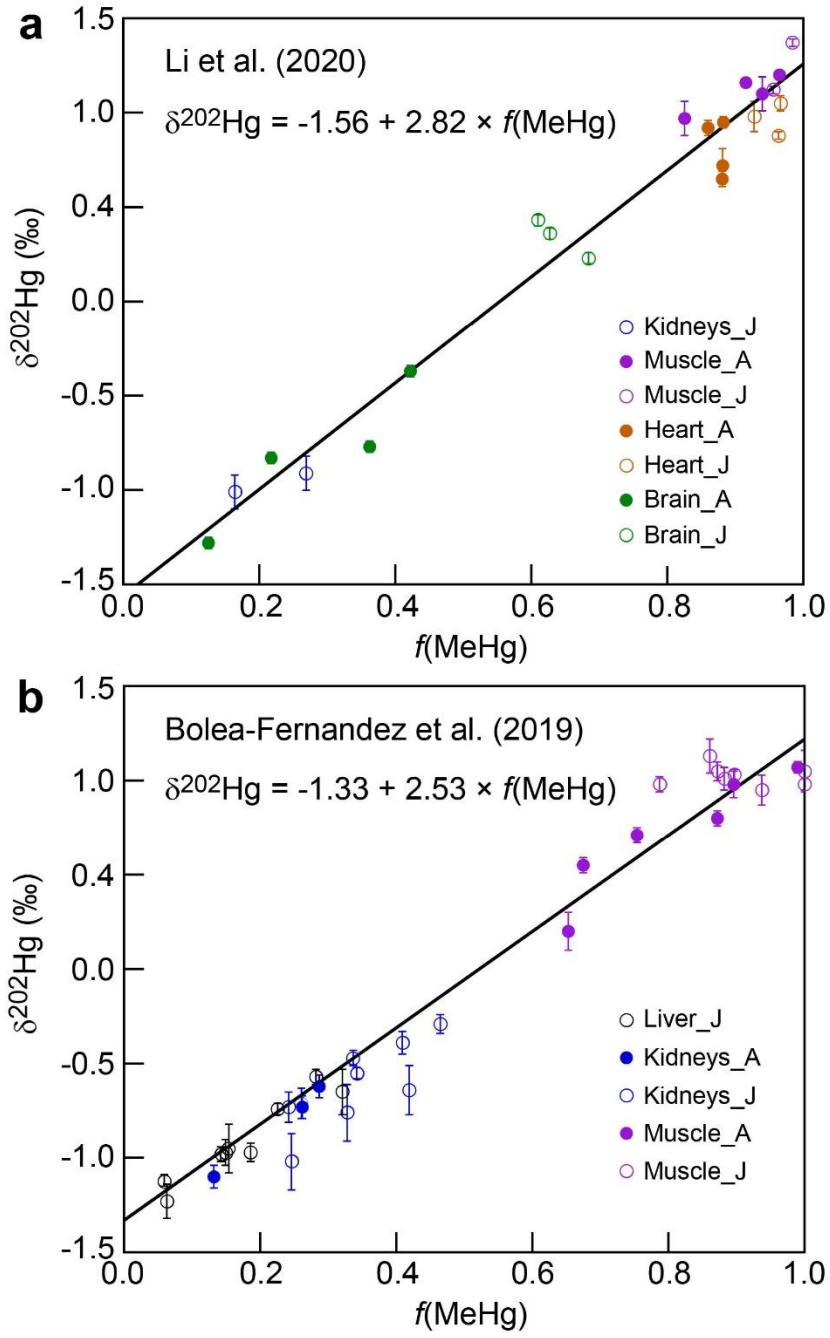
a
Li et al. (2020)
δ202Hg = -1.56 + 2.82 × f(MeHg)
δ202Hg (‰)
f(MeHg)
Kidneys_J
Muscle_A
Muscle_J
Heart_A
Heart_J
Brain_A
Brain_J
b
Bolea-Fernandez et al. (2019)
δ202Hg = -1.33 + 2.53 × f(MeHg)
δ202Hg (‰)
f(MeHg)
Liver_J
Kidneys_A
Kidneys_J
Muscle_A
Muscle_J

Figure 2

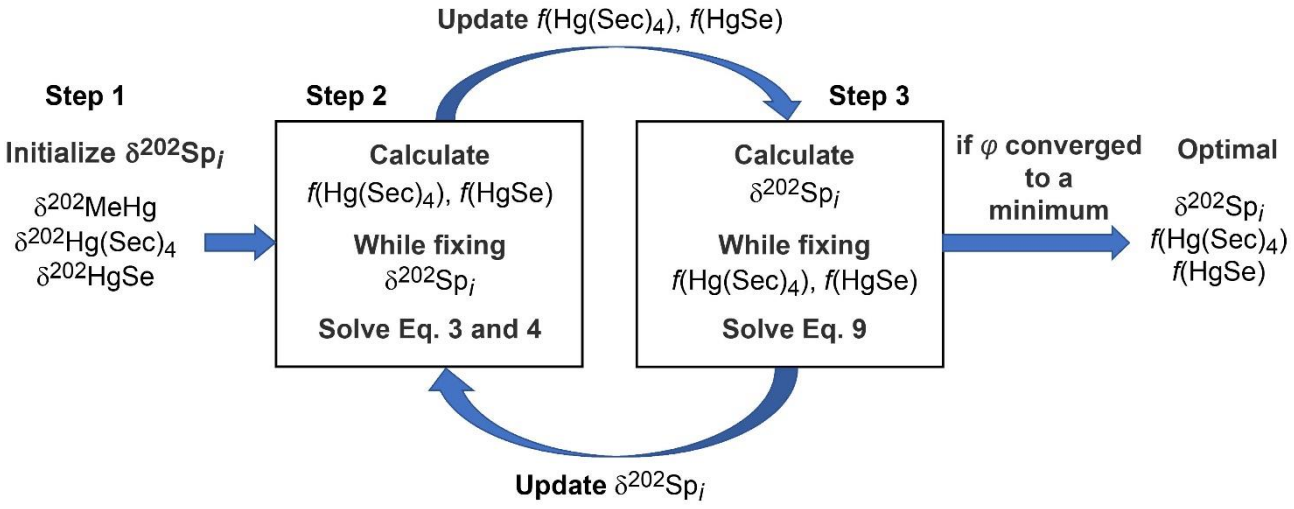

Figure 3

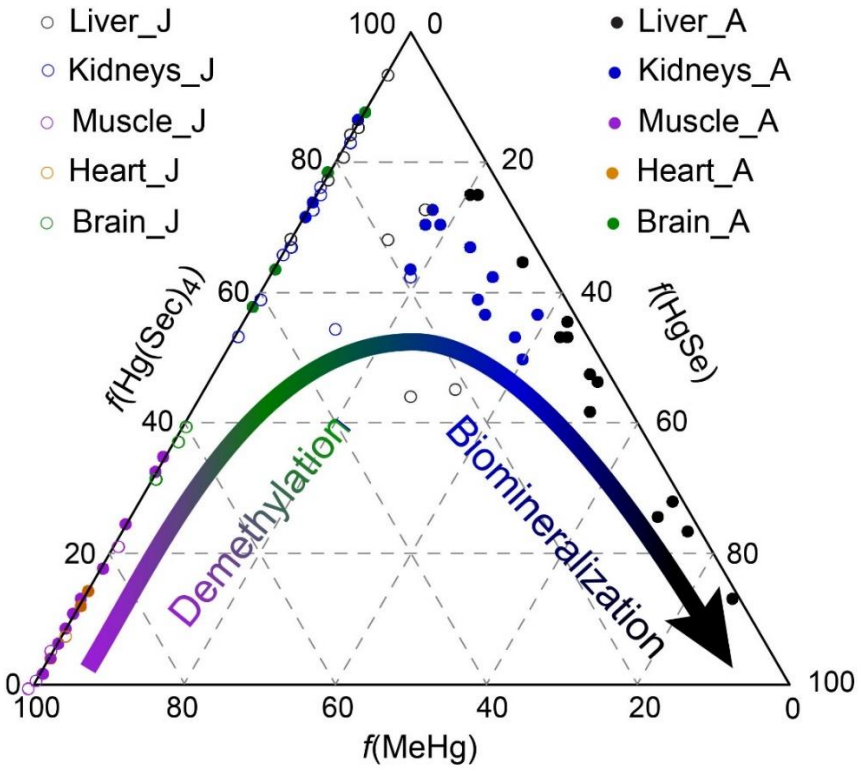

Figure 4

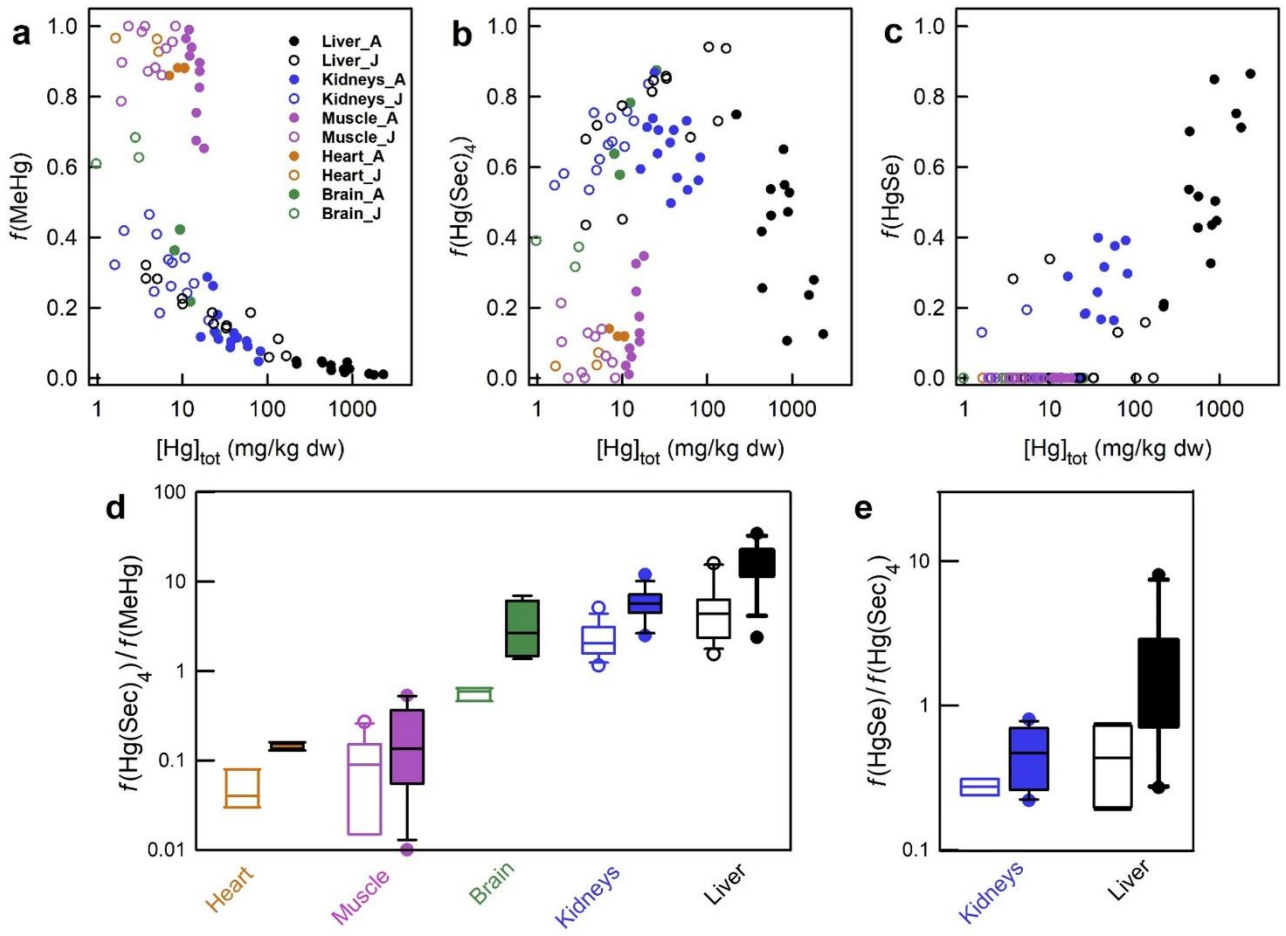
a
b
c
d
e
Liver_A
Liver_J
Kidneys_A
Kidneys_J
Muscle_A
Muscle_J
Heart_A
Heart_J
Brain_A
Brain_J
f(MeHg)
f(Hg(Sec)4)
f(HgSe)
[Hg]tot (mg/kg dw)
f(Hg(Sec)4)/f(MeHg)
f(HgSe)/f(Hg(Sec)4)
Heart
Muscle
Brain
Kidneys
Liver

Figure 5

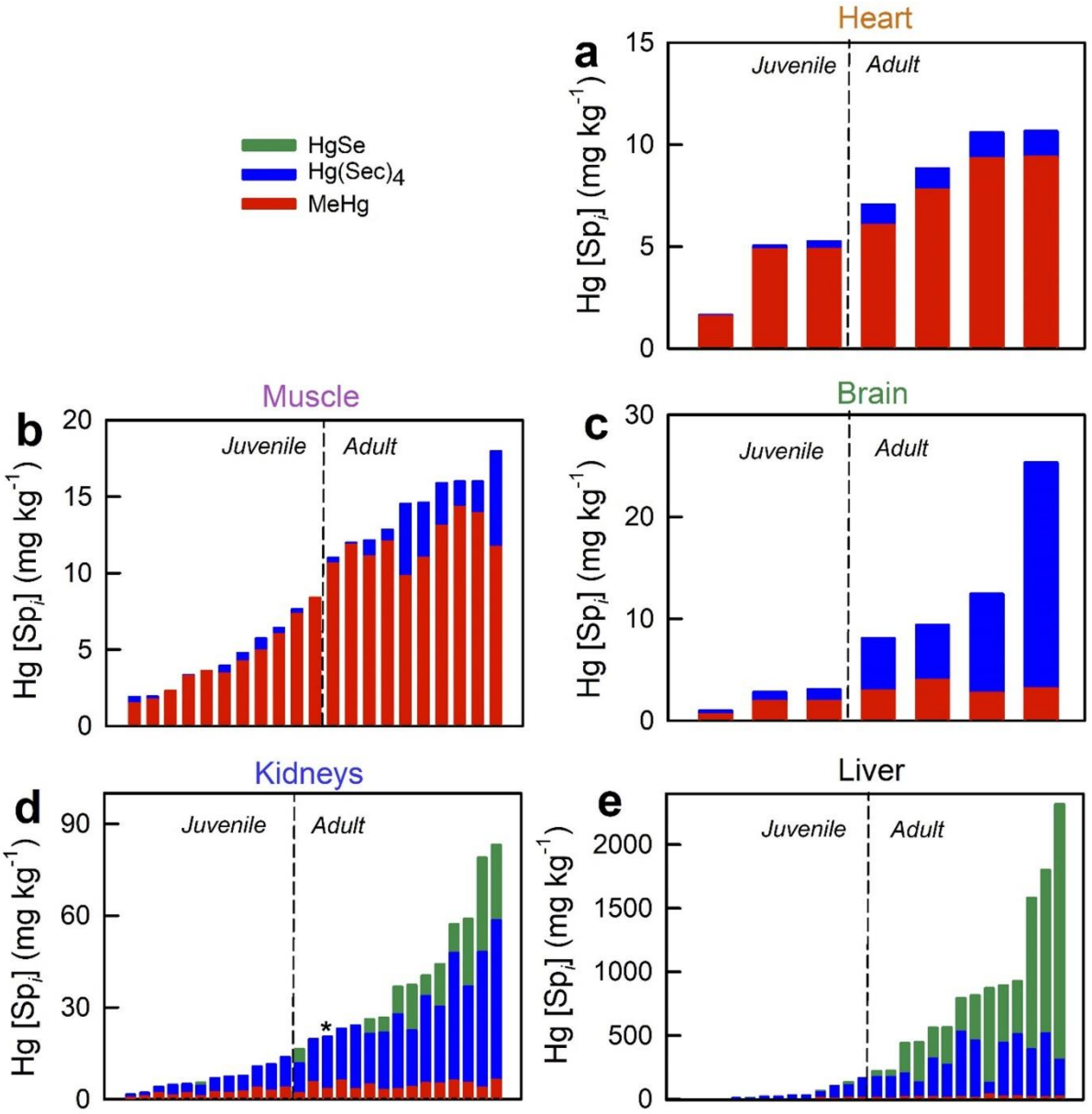
HgSe
Hg(Sec)4
MeHg
a
Heart
Juvenile
Adult
Hg [Spj] (mg kg-1)
b
Muscle
c
Brain
d
Kidneys
e
Liver
*

Figure 6

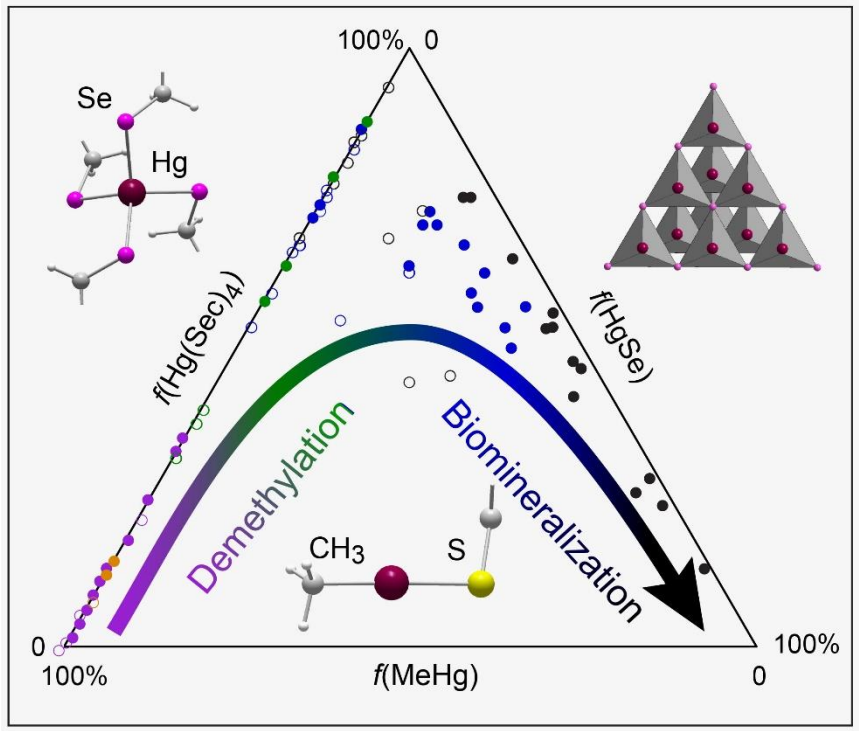
100%
0
Se
Hg
f(Hg(Sec)4)
f(HgSe)
Demethylation
Biomineralization
CH3
S
0
100%
100%
f(MeHg)
0

TOC